Strong noise-tolerant deep learning network for automatic microseismic events classification

Jian He[1,1], Huailiang Li[1,1], Xianguo Tuo[1,1], Xiaotao Wen[1,1], Wenzheng Rong[1,1], and Xin He[1,1]

[1]Chengdu University of Technology

November 30, 2022

Abstract

Identifying useful microseismic events is one of the key steps in monitoring tunnel rockbursts. Here, we propose a strong noise-tolerant deep learning (SNTDL) network for the automatic classification of noisy microseismic events. First, to comprehensively characterize the microseismic events, we extract nine weakly correlated features of the microseismic recordings as the input of training the SNTDL network. Then, a jump connection and concatenation structure are added to this network, which can further enhances its generalization ability. Additionally, the SNTDL, AlexNet, Inception, Visual Geometry Group, and ResNet are compared using the synthetic microseismic recordings with different signal-noise ratios. The results demonstrate that the SNTDL network has a higher accuracy and stronger noise-tolerant capability than the other approaches. Application to a dataset collected from a different construction environment confirms that the SNTDL network can still achieve an accurate classification result, which further verifies that the proposed network has a reliable generalization performance.

Highlights

Strong noise-tolerant deep learning network for automatic microseismic events classification

Jian He,Huailiang Li,Xianguo Tuo,Xiaotao Wen,Wenzheng Rong,Xin He

- A deep learning network using the jump connection and concatenation structure for noisy microseismic events classification was proposed.

- The developed network can accurately distinguish the noise signals and useful microseismic events with different signal-noise ratios.

- Network training by using multiple features extracted from unfiltered datasets can enhance its noise-tolerant and generalization ability.

Strong noise-tolerant deep learning network for automatic microseismic events classification

Jian He[a,b], Huailiang Li[a,b,*], Xianguo Tuo[b], Xiaotao Wen[a,b], Wenzheng Rong[a,b] and Xin He[c]

[a]*Key Laboratory of Earth Exploration and Information Technology, Ministry of Education, Chengdu University of Technology, ChengDu, 610059, Sichuan, China*

[b]*State Key Laboratory of Geohazard Prevention and Geoenvironment Protection, Chengdu University of Technology, ChengDu, 610059, Sichuan, China*

[c]*School of Mechanical and Electrical Engineering, Chengdu University of Technology, ChengDu, 610059, Sichuan, China*

ARTICLE INFO

ABSTRACT

Identifying useful microseismic events is one of the key steps in monitoring tunnel rockbursts. Here, we propose a strong noise-tolerant deep learning (SNTDL) network for the automatic classification of noisy microseismic events. The training set, validation set, and test set of the SNTDL network consist of 27,989 unfiltered microseismic recordings First, to comprehensively characterize the microseismic events, we extract nine weakly correlated features of the microseismic recordings as the input of training the SNTDL network. Then, a jump connection and concatenation structure are added to this network, which can further enhances its generalization ability. Additionally, the SNTDL, AlexNet, Inception, Visual Geometry Group, and ResNet are compared using the synthetic microseismic recordings with different signal-noise ratios. The results demonstrate that the SNTDL network has a higher accuracy and stronger noise-tolerant capability than the other approaches. Application to a dataset collected from a different construction environment confirms that the SNTDL network can still achieve an accurate classification result, which further verifies that the proposed network has a reliable generalization performance.

1. Introduction

Identifying useful microseismic events is the primary task in rockburst monitoring Zheng, Lu, Peng and Jiang (2018); Johnson, Ben-Zion, Meng and Vernon (2020). Owing to the complexity of the underground construction environment (e.g., tunnel excavation and mining engineering), the microseismic monitoring systems are usually contaminated by different vibration sources, such as explosives, machinery, vehicles, and electronics Tang, Zhao, Li and Zhu (2018); Peng, He, Wang and Jiang (2020); Jiang, Dai, Liu and Li (2021). Various types of denoising methods have been developed to suppress the random noise with microseismic recordings, such as the Kalman filter Chen, Zhang and Eaton (2020), frequency domain filtering Azarov, Serdyukov and Gapeev (2020), template matching algorithms Mu, Lee and Chen (2017); Skoumal, Brudzinski, Currie and Levy (2014), wavelet transformation Li, Tuo, Wang and Courtois (2019), empirical and variation mode decomposition Gómez and Velis (2016); Zhang, Dong and Xu (2020), and fingerprint and similarity threshold algorithms Yoon, O'Reilly, Bergen and Beroza (2015); Bergen and Beroza (2019). These approaches have played an important role in different application fields and are still frequently applied. However, these methods have difficulty reducing the random noise that shares a common frequency band with the useful microseismic events Zhu, Mousavi and Beroza (2019). In addition, it is also difficult for operators with extensive professional knowledge and experience to accurately select useful microseismic events from a series of similar microseismic waveforms Dong, Wesseloo, Potvin and Li (2016).

In recent years, researchers have gradually paid more attention to the use of machine learning to analyze massive amounts of seismic data Rouet-Leduc, Hulbert, Lubbers, Barros, Humphreys and Johnson (2017); Corbi, Sandri, Bedford, Funiciello, Brizzi, Rosenau and Lallemand (2019); Bergen, Johnson, Maarten and Beroza (2019); Mousavi and Beroza (2020). In addition, serval algorithms have been increasingly used to identify the microseismic events, such as extreme learning machines Zhang, Jiang, Li and Xu (2019), the Gaussian mixture model Wang, Tang, Ma, Wang and Li (2020), logistic regression Pu, Apel and Hall (2020), the random forest algorithm Provost, Hibert and Malet (2017), and neural network algorithms Xu, Zhang, Chen, Li and Liu (2021). Although these studies have laid the foundation for the development of microseismic data processing, there is still a large gap regarding the demand for efficient, accurate, and real-time identification of useful microseismic events for engineering applications.

In addition, the popular convolutional neural networks (CNN) has been widely applied to extract low-, medium- and high-level features from input data using convolution calculations, which can significantly improve the pre-processing efficiency of the input data LeCun, Bengio and Hinton (2015); Afshari Moein, Tormann, Valley and Wiemer (2018); Liu, Zhang, Zhu, Ellsworth and Li (2020); Shokouhi, Girkar, Riviere, Shreedharan, Marone, Giles and Kifer (2021). With the growing interest in improved CNNs, numerous alternative CNN techniques have been developed for the microseismic monitoring applications, especially for microseismic event recognition strategies. Wilkins, Strange, Duan and Luo (2020) trained a CNN using a large number of mine microseismic datasets and further demonstrated that this CNN can achieve a better accuracy than experienced

*Corresponding author
✉ lihl@cdut.edu.cn (H. Li)

seismic experts. Tang, Wang and Tang (2021) successfully identified single-channel and multi-channel microseismic events based on a CNN architecture constructed using the residual skip connections and an attention mechanism. Bi, Zhang, He, Zhao, Sun and Ma (2021) built a deep CNN that learns the features of microseismic events from the time domain and frequency domain based on a dual-channel classification module and interpretation module, and verified the effectiveness of this CNN method. The aforementioned methods can effectively improve the accuracy and reliability of microseismic event classification when applied to high quality datasets (usually, the input data need to be filtered), but there is room for improvement in classifying noisy microseismic datasets, particularly for the microseismic recordings with high-noise from the complex engineering environments.

In this study, we developed and evaluated a strong noise-tolerant deep learning (SNTDL) network, which can identify noisy microseismic events in complex tunnel construction environments. We verified the contributions of the selected features based on the classification precision, recall, F1-score, and accuracy of the SNTDL network. Furthermore, to test the performance of the proposed SNTDL network, we compared the classification results of our method with the results obtained using the AlexNet Krizhevsky, Sutskever and Hinton (2012), Inception Szegedy, Liu, Jia, Sermanet, Reed, Anguelov, Erhan, Vanhoucke and Rabinovich (2015), Visual Geometry Group (VGG) Simonyan and Zisserman (2014), and ResNet He, Zhang, Ren and Sun (2016) approaches.

2. Dataset

2.1. Feature Extraction

The dataset used consists of microseismic events, blast signals, mechanical noise, and electromagnetic interference signals, which were collected from a deeply buried tunnel excavation monitoring project. The sample rate of the microseismic monitoring system was set to 12,000 Hz. Our primary purpose was to monitor the stability of the rock masses and provide a warning of rockburst events in this microseismic monitoring work. Thus, we divided all of the recordings into two categories: useful microseismic events and the other noise signals. Based on the time domain and frequency domain characteristics of the collected data, the dataset production was manually labeled, including 13,997 microseismic events and 13,992 noise recordings. We calculated the dynamic and kinematic features of the unfiltered microseismic recordings, focusing on the waveform, power, phase, time-frequency spectrum and frequency spectrum, etc. Table 1 shows the methods of calculating the 10 commonly used features.

As is shown in Table 1, the normalization of the waveform is conducted to reduce the numerical difference at each sample point. Hilbert's marginal spectrum accurately reflects the actual frequency compositions of the non-stationary signals and characterizes the cumulative amplitude distribution of the entire dataset at each frequency point Huang,

Wu, Qu, Long and Shen (2003); Fan, Zhang, Zhang and Ouyang (2017). The energy ratio is helpful in analyzing the energy changes before and after the arrival of the seismic waves Mousa, Al-Shuhail and Al-Lehyani (2011). The instantaneous power is also the most important statistical indicator of random vibration signals Zengin and Abrahamson (2020). The Akaike information criterion (AIC) is a standard used to determine the fitting performance of a statistical model Zhang, Thurber and Rowe (2003). The frequency spectrum curve represents the trigonometric function component of the specified frequency, and it can reflects the frequency compositions of the stationary signal. The phase spectrum reflects the relationship between the phase and frequency Meng, Guo, Zhang, Li and Zhou (2008). The instantaneous amplitude, instantaneous phase, and instantaneous frequency reflect that the changes in the amplitude, phase, and frequency with time, respectively. Shoji, Miyoshi, Omura, Kistler, Kasaba, Matsuda, Kasahara, Matsuoka, Nomura, Ishisaka et al. (2018); Mousavi, Holloway, Olivier and Gandomi (2021).

2.2. Feature Selection

Adding similar features will produce information redundancy when there is a strong correlation between the various features, which will result in overfitting of the training model. Regarding the correlation verification, the classic Pearson correlation coefficient can be used to effectively determine the interrelationship between two variables, but it is only a linear measurement method and has difficulty authentically reflecting the interdependence between different variables Saccenti, Hendriks and Smilde (2020). Therefore, the Spearman correlation coefficient was used to determine the correlation between two features, which has the advantages of not being affected by the data's dimensions and not being sensitive to abnormal large numbers Su and Li (2021).

Usually, the greater the absolute value of the correlation coefficient is, the closer the monotonic relationship between the two features is. Table 2 presents the average correlation coefficient between each feature for 1,000 real microseismic recordings. Clearly, the instantaneous amplitude is strongly correlated with the instantaneous power and AIC. Therefore, we excluded the instantaneous amplitude feature to avoid information redundancy. Finally, a microseismic recording can be expressed as a $6,000 \times 9$ matrix which consists of the waveform, marginal spectrum, energy ratio, instantaneous power, AIC, frequency spectrum, phase spectrum, instantaneous phase, and instantaneous frequency.

3. Model Training and Evaluation

Since the Alexnet provided a new idea for deep learning network algorithms, deeper network structures have been developed rapidly. In the field of image recognition, deep residual networks that introduce substantial skip or bypass connections have been found to be more effective in mitigating the gradient vanishing He et al. (2016). Based on a

Table 1
The calculation methods and parameters for different features.

| Features	Definition	Parameters
Waveform	$x(t) = \dfrac{x_o(t) - \mu}{\sigma}$	$x(t)$ is the normalized data, $x_o(t)$ is the original data, μ is the mean of $x_o(t)$, σ is the standard deviation of $x_o(t)$.
Marginal spectrum	$h(\omega) = \int_0^T H(\omega, t)\, dt$	$h(\omega)$ is the Hilbert marginal spectrum of $x(t)$, $H(\omega, t)$ is the Hilbert spectrum of $x(t)$, and T is the time.
Energy ratio	$E = \dfrac{\left[\sum_{t=T_1}^{T_2} x^2(t)\right]^{\frac{1}{2}} + \alpha\omega}{\left[\sum_{t=T_0}^{T_1} x^2(t)\right]^{\frac{1}{2}} + \alpha\omega}$	E is the energy ratio in two time windows, $\omega = \frac{1}{N}\left[\sum_{t=0}^{T} x^2(t)\right]$ is the relative energy of the signal, N is the sample length of the signal, and α is a stability coefficient.
Instantaneous power	$IP = |x(t)|^2$	IP is the instantaneous power of $x(t)$.
Akaike information criterion	$AIC(k) = k \log\{\mathrm{var}[x(1,k)]\}$ $+ (N - k - 1)\log\{\mathrm{var}[x(k+1,N)]\}$	AIC is a statistical measure for estimating the quality of time series models fitting. $k = 1, 2, \ldots, N$, var represents variance calculation.
Frequency spectrum	$FS = \dfrac{|F(\omega)|}{N}$	FS is the frequency spectrum of $x(t)$, and $F(\omega)$ is the image function obtained by using the Fourier transform of $x(t)$.
Phase spectrum	$PS = \arctan(F(\omega))$	PS is the phase spectrum of $x(t)$.
Instantaneous amplitude	$\alpha(t) = \sqrt{x^2(t) + h^2(t)}$	$\alpha(t)$ is the instantaneous amplitude of $x(t)$, and $h(t)$ is the imaginary part produced by using the Hilbert transformation.
Instantaneous phase	$\varphi(t) = \arctan\dfrac{h(t)}{x(t)}$	$\varphi(t)$ is the instantaneous phase of $x(t)$.
Instantaneous frequency	$\omega(t) = \dfrac{d\varphi(t)}{dt}$	$\omega(t)$ is the instantaneous frequency of $x(t)$.

Table 2
The correlation coefficient between two different features.

Feature	waveform	$h(\omega)$	E	IP	AIC	FS	PS	$\alpha(t)$	$\varphi(t)$	$\omega(t)$
waveform	1.0000	0.0051	0.0220	0.0008	0.0131	0.0178	0.0016	0.0108	0.0078	0.1247
$h(\omega)$		1.0000	0.0212	0.1300	0.2972	0.2348	0.0058	0.1920	0.0247	0.1185
E			1.0000	0.0090	0.0158	0.0012	0.0161	0.0055	0.1563	0.0052
IP				1.0000	0.2611	0.1428	0.0108	0.7819	0.0013	0.1044
AIC					1.0000	0.2676	0.0039	0.7777	0.0025	0.1796
FS						1.0000	0.0065	0.3356	0.0178	0.1277
PS							1.0000	0.0096	0.0034	0.0181
$\alpha(t)$								1.0000	0.0086	0.0664
$\varphi(t)$									1.0000	0.2892
$\omega(t)$										1.0000

CNN, the ResNet is usually composed of input, output, convolution, pooling, activation, straightening, and fully connected layers O'Shea, Roy and Clancy (2018). The SNTDL model proposed in this study is a derivation of the ResNet. Figure 1(a) illustrates the residual unit of the trained SNTDL network, which consists of convolution, maximum pooling, skip connection and concatenation structure. Figure 1(b) shows a residual block, including two residual units. Figure 1(c) shows the detailed structure of the SNTDL network, which consists of 4 residual blocks and 6,871,762 parameters. The ReLu activation function is used to increase the sparsity of the neural network and the nonlinear relationship between the different layers. A drop operation is also used between the two fully connected layers, which resulted in 50% of the neurons being dormant. In addition, we chose the Adam optimizer to guide the network and update the parameters during the training process. The initial learning rate was set to 0.001. The learning rate of the optimizer decreases as the number of iterations increases.

We randomly subdivided the 27,989 microseismic recordings collected from the Grand Canyon Tunnel into a training set, validation set, and test set, which accounted for 80%,
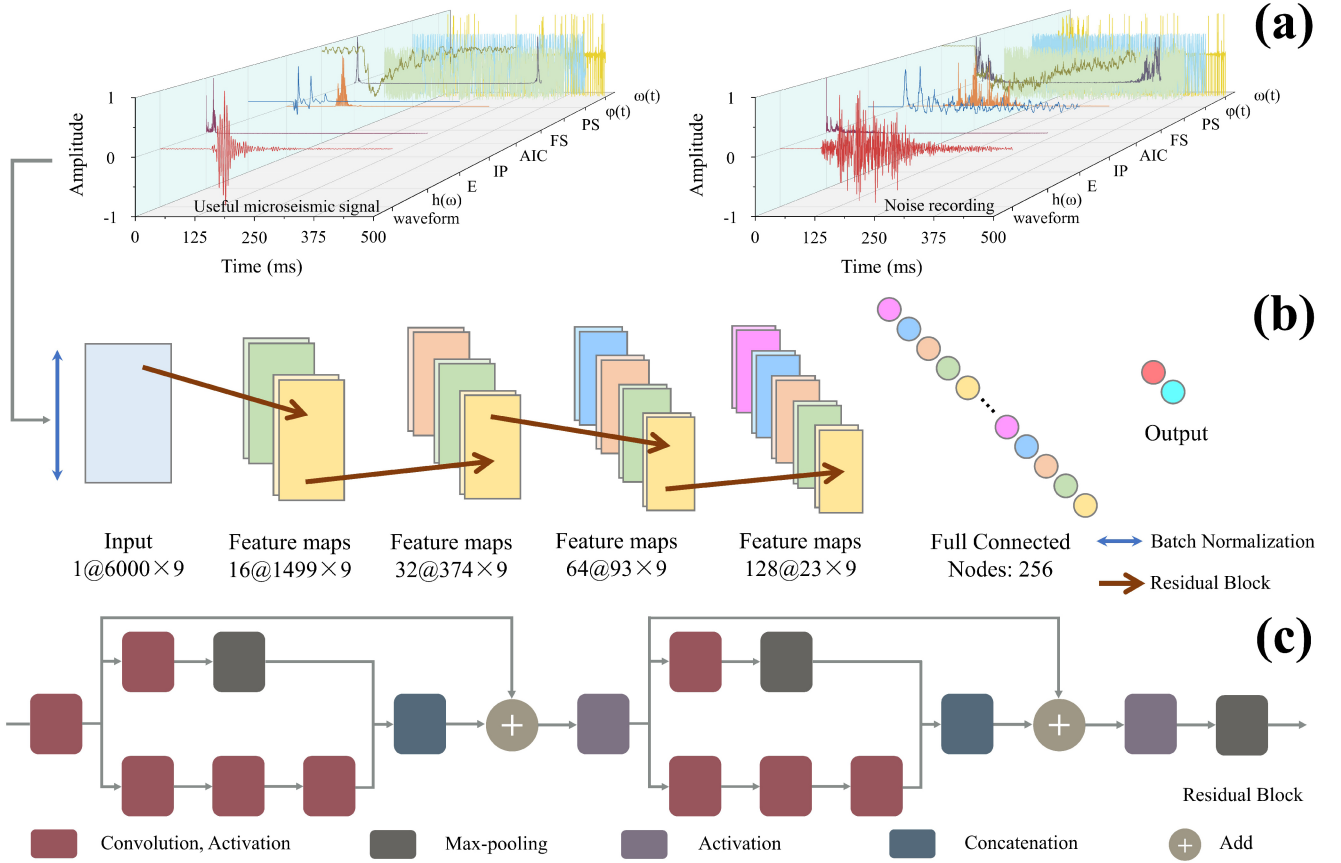
Figure 1: The detailed structure diagram of the proposed SNTDL network. (a) A single-channel recording with a duration of 500ms, the corresponding features of the useful microseismic signal are shown on the left subgraph, and those of the noisy recording are shown on the right subgraph; (b) the structure of the SNTDL network, the residual block is used to extract the deep features, and the final full connected layers is applied to determine that the received signal is or not a useful microseismic signal; (c) the residual block used in the SNTDL network, which includes convolution, pooling, concatenation and residual units.

10%, and 10% of the entire dataset, respectively Saad, Huang, Chen, Savvaidis, Fomel, Pham and Chen (2021). As is shown in Figure 2(a), the entire training process was accomplished by performing 150 epochs. The validation accuracy increased from 74.1% to 98.3%, and the loss decreased from 0.52 to 0.05. The SNTDL network exhibited a good stability during the training process, and no over-fitting phenomenon occurred.

The test set consisted of 1,400 valid microseismic event recordings and 1,399 noise recordings. We evaluated the ability of the SNTDL network to identify microseismic events based on the precision, recall, F1-score, and accuracy Mousavi, Zhu, Sheng and Beroza (2019), which are defined in Equation 1−4. As is shown in Figure 2(b), for the test set, the SNTDL network accurately classified most of the test samples, and the recognition precision, recall, and F1-score of the SNTDL network are 97.66%, 98.21%, and 97.93%, respectively. The overall recognition accuracy of the test set was 97.93%. In addition, the area under the curve (AUC) of the SNTDL model for identifying microseismic events is 0.9887, which means that the model has a robust verification performance.

$$Precision = \frac{TP}{TP + FP} \tag{1}$$

$$Recall = \frac{TP}{TP + FN} \tag{2}$$

$$F1\text{-}score = \frac{2 \times Precision \times Recall}{Precision + Recall} \tag{3}$$

$$Accuracy = \frac{TP + TN}{TP + TN + FP + FN} \tag{4}$$

in which, TP and FP are the true positive and false positive, respectively, and TN and FN are the true negative and false negative, respectively.

4. Results and Discussion

4.1. Feature Contributions

We designed a set of experiments to confirm that each of the aforementioned nine features made a definite contribution to the final prediction results of the SNTDL network

(a)

(b)
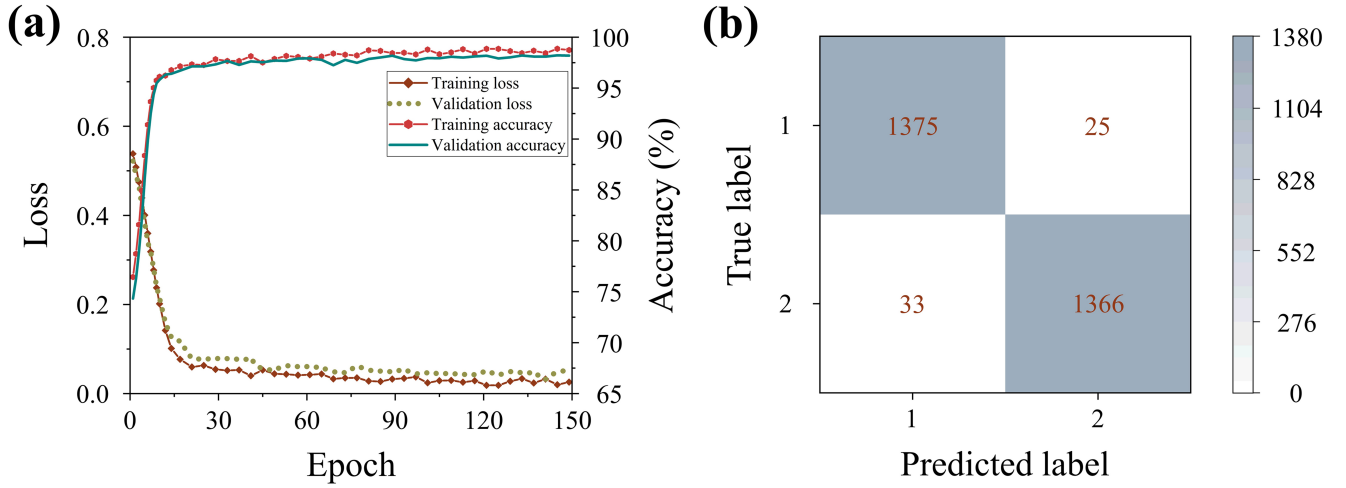
Figure 2: Training process and test results of the SNTDL network. (a) Accuracy and loss varying with epochs during the SNTDL network training; (b) confusion matrix obtained from the test results of the SNTDL network.

because there are too many input features in the proposed SNTDL network. Only one feature was extracted from the input during the training of the SNTDL network, and the corresponding input of the validation set and test set also contained only one correlated feature. The classification results are shown in Figure 3(a), in which the horizontal coordinates indicate the used features contained in the training set, validation set, and test set for each experiment. As can be seen from the calculated recognition precision, recall, F1-score, and accuracy, each of the extracted nine features made significant and different contributions to the proposed SNTDL network. Then, we constructed a new training set, including eight features, as the input to train the SNTDL network. The eight selected features are obtained by successively removing one feature from the aforementioned nine features, and the corresponding input of the validation set and test set also consisted of the correlated eight features. The classification results are shown in Figure 3(b), and the removed feature corresponds to the Figure 3(a). As can be seen from Figure 3, if one of the nine features in Figure 3(a) yields a better classification result, it will produce a worse classification result so this corresponding feature was removed in Figure 3(b). Thus, this feature made a larger contribution to the SNTDL network. In this sense, the waveform feature and Hilbert marginal spectrum feature have the greatest impacts on the classification results, followed by the instantaneous power, AIC, and frequency spectrum features.

4.2. Noise-tolerant Performance

To verify the noise-tolerant performance of the SNTDL network, we constructed 17 test sets by adding the white Gaussian noise to the synthetic microseismic recordings with different signal-to-noise ratios (SNRs), and the corresponding SNRs were set within the range of -12 dB to 20 dB. The 17 constructed test sets were used to compare the SNTDL network with other popular deep learning networks, including the 8-layer AlexNet, 10-layer Inception, 16-layer

VGG, and 18-layer ResNet. As is shown in Figure 4(a), the classification precisions of the AlexNet, Inception, VGG, and ResNet are close to zero while their SNRs are set between -12 dB and -6 dB, due to that these networks wrongly identified the useful signals as noise. As can be seen from Figure 4(b), when the SNR was set to -2 dB, the recall of the useful microseismic events for the proposed SNTDL network was 87.8%, the recalls of the AlexNet, Inception, VGG, and ResNet were 1.5%, 1.4%, 1.9%, and 4.1%, respectively. In addition, as is shown in Figure 4(c) and Figure 4(d), when the SNR was reduced to -4 dB, the F1-score and the accuracy of the SNTDL network were still 90%. Moreover, the recall of the SNTDL network was still 1.9% until that the SNR decreased to -12 dB, which further confirms that the SNTDL network has a better noise-tolerant performance than the other networks.

4.3. Generalization

To verify the generalization ability of the proposed SNTDL network, we applied the SNTDL network to a series of microseismic recordings, which were collected from a different underground tunnel excavation monitoring project. These microseismic recordings were manually marked to form a dataset containing 1,000 useful microseismic events and 1,000 noise signals. The data acquisition system used was same as that of the aforementioned training microseismic recordings, but the sample rate was different (6000 Hz). Additionally, the construction machinery and TNT equivalent used in the two construction regions were also different. We used the SNTDL network to classify these subdivided microseismic recordings and compare the predicted label with the real subdivided label. If the predicted label was consistent with the real label, the detection result was regarded as a true positive; otherwise, it was regarded as a false positive. As a result, the SNTDL network successfully distinguished 1,912 events, including 963 useful microseismic events and 949 noise signals. Furthermore, for
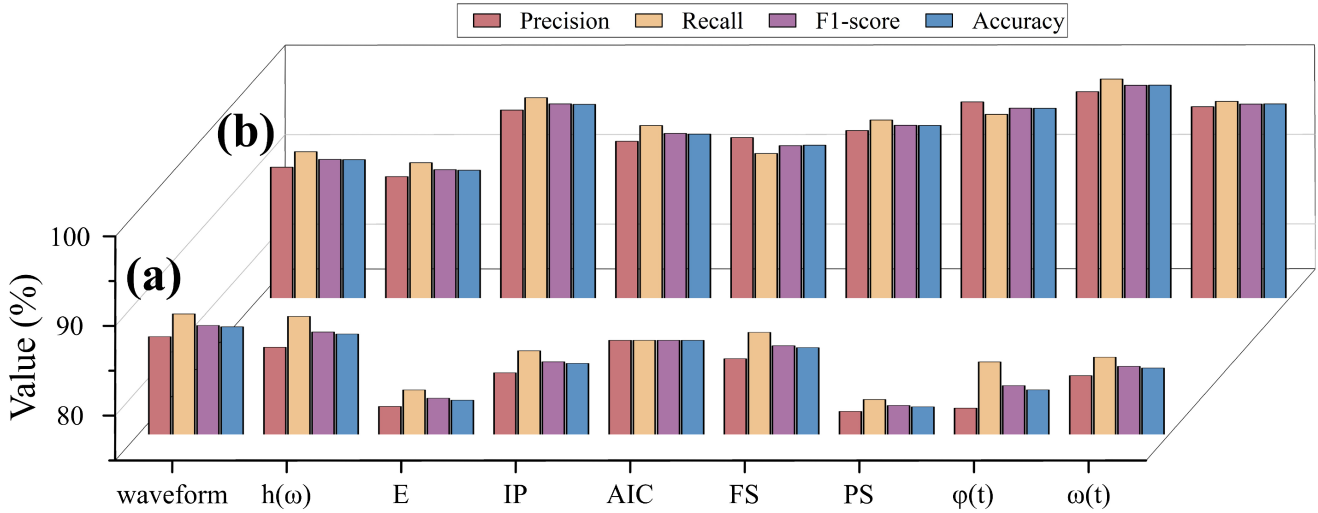
Figure 3: The contribution of each feature in the training dataset for the recognition of microseismic events by using the SNTDL network. (a) The classification precision, recall, F1-score, and accuracy of the SNTDL network while using only one feature in the training dataset; (b) the classification precision, recall, F1-score, and accuracy of the SNTDL network while removing one feature in the training dataset.

this labeled dataset, the classification precision, recall, F1-score, and accuracy of the SNTDL network were 94.97%, 96.30%, 95.63%, and 95.60%, respectively. In this sense, the proposed SNTDL network can keep a reliabe identification performance for different microseismic recordings, which further reveals that the SNTDL network has a favorable generalization ability.

5. Conclusions

In this study, a strong noise-tolerant deep learning (SNTDL) network for classifying the noisy microseismic recordings was proposed. To enhance the noise-tolerant ability of the proposed SNTDL network, we extracted nine weakly correlated features of the microseismic recording as the training input of the SNTDL network instead of the original microseismic recordings. In addition, we also confirmed that each of the used nine features used made a definite contribution to the final classification results of the proposed SNTDL network. Moreover, the added skip connection, concatenation structure, and deep structure of 6,871,762 parameters also improved the noise-tolerant performance while training the SNTDL network. We compared the noise-tolerant ability of the proposed SNTDL with those of the AlexNet, Inception, VGG, and ResNet, and the results indicate that the proposed SNTDL has a better noise-tolerant performance. Furthermore, the corresponding classification F1-score and the accuracy are still 90%, while the SNR is reduced to -4 dB. We applied the proposed SNTDL network to a series of completely independent and labeled microseismic recordings, and the SNTDL network still achieved an accurate classification result, which further verifies that the SNTDL network has a favorable generalization performance. In summary, the proposed SNTDL network

can provide a robust classification of noisy microseismic recordings, which can make a significant contribution to the real-time monitoring of microseismic events.

CRediT authorship contribution statement

Jian He: Writing - original draft, Software, Investigation, Methodology. Huailiang Li: Writing - review & editing, Conceptualization, Resources, Supervision. Xianguo Tuo: Validation, Writing - review & editing. Xiaotao Wen: Writing - review & editing, Validation. Wenzheng Rong: Writing - original draft, Software. Xin He: Investigation, Methodology.

Declaration of Competing Interest

The authors declare that they have no known competing financial interests or personal relationships that could have appeared to influence the work reported in this paper.

Acknowledgments

References

Afshari Moein, M.J., Tormann, T., Valley, B., Wiemer, S., 2018. Maximum magnitude forecast in hydraulic stimulation based on clustering and size distribution of early microseismicity. Geophysical Research Letters 45, 6907–6917.

Azarov, A.V., Serdyukov, A.S., Gapeev, D.N., 2020. Research note: Frequency domain orthogonal projection filtration of surface microseismic monitoring data. Geophysical Prospecting 68, 382–392.
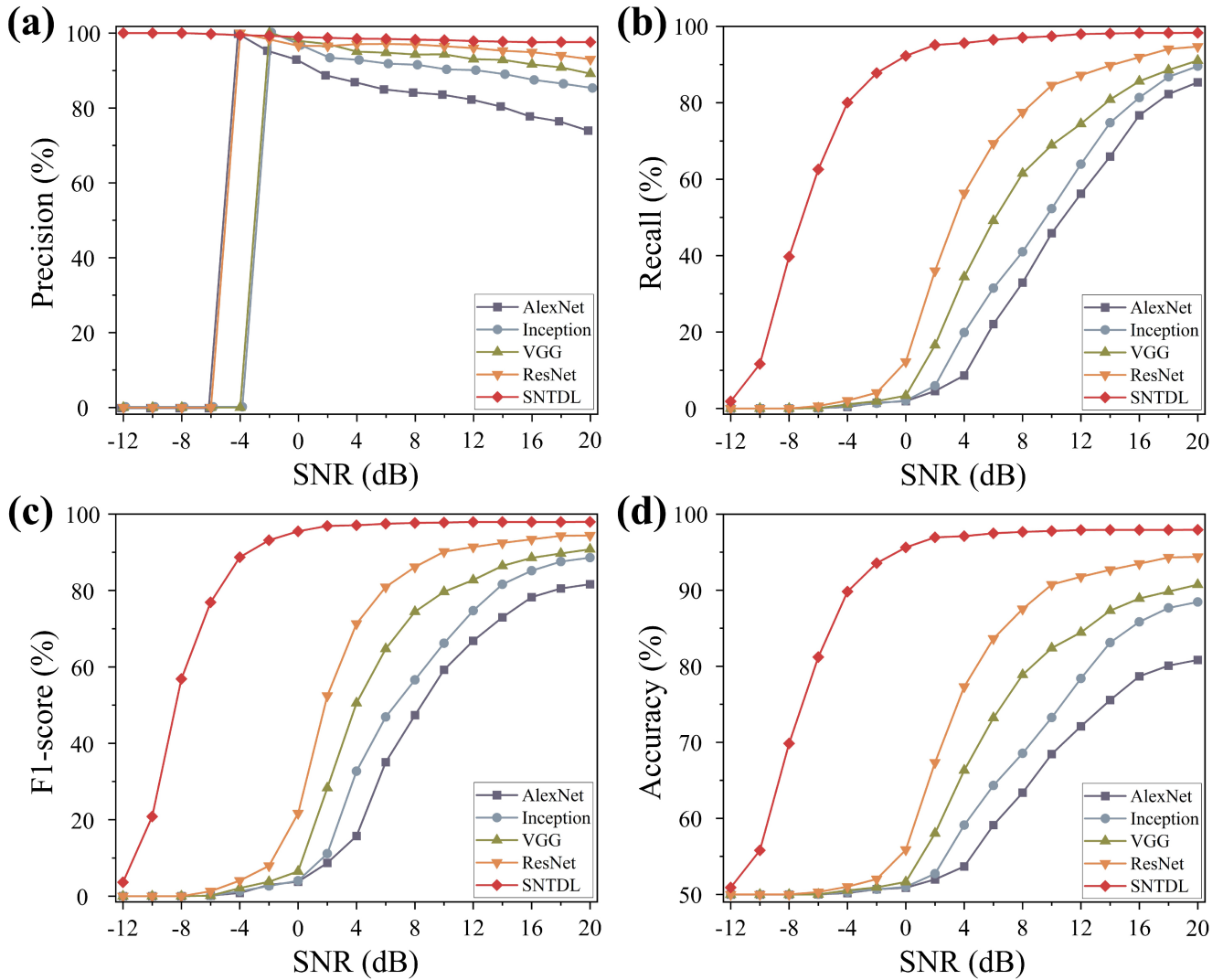
Figure 4: Noise-tolerant performance comparison of the SNTDL, AlexNet, Inception, VGG, and ResNet networks using the synthetic microseismic datasets with different SNRs. (a) Identification precision of different classification networks; (b) identification recall of different classification networks; (c) identification F1-score of different classification networks, which is used to eliminate the effect of unbalanced sample sizes for different networks; (d) identification accuracy of different classification networks.

Bergen, K.J., Beroza, G.C., 2019. Earthquake fingerprints: Extracting waveform features for similarity-based earthquake detection. Pure and Applied Geophysics 176, 1037–1059.

Bergen, K.J., Johnson, P.A., Maarten, V., Beroza, G.C., 2019. Machine learning for data-driven discovery in solid earth geoscience. Science 363.

Bi, X., Zhang, C., He, Y., Zhao, X., Sun, Y., Ma, Y., 2021. Explainable time–frequency convolutional neural network for microseismic waveform classification. Information Sciences 546, 883–896.

Chen, Y., Zhang, H., Eaton, D.W., 2020. Real-time earthquake location based on the kalman filter formulation. Geophysical Research Letters 47, e2019GL086240.

Corbi, F., Sandri, L., Bedford, J., Funiciello, F., Brizzi, S., Rosenau, M., Lallemand, S., 2019. Machine learning can predict the timing and size of analog earthquakes. Geophysical Research Letters 46, 1303–1311.

Dong, L., Wesseloo, J., Potvin, Y., Li, X., 2016. Discrimination of mine seismic events and blasts using the fisher classifier, naive bayesian classifier and logistic regression. Rock Mechanics and Rock Engineering 49, 183–211.

Fan, G., Zhang, L.M., Zhang, J.J., Ouyang, F., 2017. Energy-based analysis of mechanisms of earthquake-induced landslide using hilbert–huang transform and marginal spectrum. Rock Mechanics and Rock Engineering 50, 2425–2441.

Gómez, J.L., Velis, D.R., 2016. A simple method inspired by empirical mode decomposition for denoising seismic data. Geophysics 81, V403–V413.

He, K., Zhang, X., Ren, S., Sun, J., 2016. Deep residual learning for image recognition, in: Proceedings of the IEEE conference on computer vision and pattern recognition, pp. 770–778.

Huang, N.E., Wu, M.L., Qu, W., Long, S.R., Shen, S.S., 2003. Applications of hilbert–huang transform to non-stationary financial time series analysis. Applied stochastic models in business and industry 19, 245–268.

Jiang, R., Dai, F., Liu, Y., Li, A., 2021. A novel method for automatic identification of rock fracture signals in microseismic monitoring. Measurement 175, 109129.

Johnson, C.W., Ben-Zion, Y., Meng, H., Vernon, F., 2020. Identifying different classes of seismic noise signals using unsupervised learning. Geophysical Research Letters 47, e2020GL088353.

Krizhevsky, A., Sutskever, I., Hinton, G.E., 2012. Imagenet classification with deep convolutional neural networks. Advances in neural information processing systems 25, 1097–1105.

LeCun, Y., Bengio, Y., Hinton, G., 2015. Deep learning. nature 521, 436–444.

Li, H., Tuo, X., Wang, R., Courtois, J., 2019. A reliable strategy for improving automatic first-arrival picking of high-noise three-component microseismic data. Seismological Research Letters 90, 1336–1345.

Liu, M., Zhang, M., Zhu, W., Ellsworth, W.L., Li, H., 2020. Rapid characterization of the july 2019 ridgecrest, california, earthquake sequence from raw seismic data using machine-learning phase picker. Geophysical Research Letters 47, e2019GL086189.

Meng, X., Guo, L., Zhang, Z., Li, S., Zhou, J., 2008. Reconstruction of seismic data with least squares inversion based on nonuniform fast fourier transform. Chinese Journal of Geophysics 51, 168–175.

Mousa, W.A., Al-Shuhail, A.A., Al-Lehyani, A., 2011. A new technique for first-arrival picking of refracted seismic data based on digital image segmentation. Geophysics 76, V79–V89.

Mousavi, M., Holloway, D., Olivier, J., Gandomi, A.H., 2021. Beam damage detection using synchronisation of peaks in instantaneous frequency and amplitude of vibration data. Measurement 168, 108297.

Mousavi, S.M., Beroza, G.C., 2020. A machine-learning approach for earthquake magnitude estimation. Geophysical Research Letters 47, e2019GL085976.

Mousavi, S.M., Zhu, W., Sheng, Y., Beroza, G.C., 2019. Cred: A deep residual network of convolutional and recurrent units for earthquake signal detection. Scientific reports 9, 1–14.

Mu, D., Lee, E.J., Chen, P., 2017. Rapid earthquake detection through gpu-based template matching. Computers & Geosciences 109, 305–314.

O'Shea, T.J., Roy, T., Clancy, T.C., 2018. Over-the-air deep learning based radio signal classification. IEEE Journal of Selected Topics in Signal Processing 12, 168–179.

Peng, P., He, Z., Wang, L., Jiang, Y., 2020. Microseismic records classification using capsule network with limited training samples in underground mining. Scientific Reports 10, 1–16.

Provost, F., Hibert, C., Malet, J.P., 2017. Automatic classification of endogenous landslide seismicity using the random forest supervised classifier. Geophysical Research Letters 44, 113–120.

Pu, Y., Apel, D.B., Hall, R., 2020. Using machine learning approach for microseismic events recognition in underground excavations: Comparison of ten frequently-used models. Engineering Geology 268, 105519.

Rouet-Leduc, B., Hulbert, C., Lubbers, N., Barros, K., Humphreys, C.J., Johnson, P.A., 2017. Machine learning predicts laboratory earthquakes. Geophysical Research Letters 44, 9276–9282.

Saad, O.M., Huang, G., Chen, Y., Savvaidis, A., Fomel, S., Pham, N., Chen, Y., 2021. Scalodeep: A highly generalized deep learning framework for real-time earthquake detection. Journal of Geophysical Research: Solid Earth 126, e2020JB021473.

Saccenti, E., Hendriks, M.H., Smilde, A.K., 2020. Corruption of the pearson correlation coefficient by measurement error and its estimation, bias, and correction under different error models. Scientific reports 10, 1–19.

Shoji, M., Miyoshi, Y., Omura, Y., Kistler, L.M., Kasaba, Y., Matsuda, S., Kasahara, Y., Matsuoka, A., Nomura, R., Ishisaka, K., et al., 2018. Instantaneous frequency analysis on nonlinear emic emissions: Arase observation. Geophysical Research Letters 45, 13–199.

Shokouhi, P., Girkar, V., Riviere, J., Shreedharan, S., Marone, C., Giles, C.L., Kifer, D., 2021. Deep learning can predict laboratory quakes from active source seismic data. Geophysical Research Letters, e2021GL093187.

Simonyan, K., Zisserman, A., 2014. Very deep convolutional networks for large-scale image recognition. arXiv preprint arXiv:1409.1556 .

Skoumal, R.J., Brudzinski, M.R., Currie, B.S., Levy, J., 2014. Optimizing multi-station earthquake template matching through re-examination of the youngstown, ohio, sequence. Earth and Planetary Science Letters 405, 274–280.

Su, L., Li, H., 2021. Project procurement method decision-making with spearman rank correlation coefficient under uncertainty circumstances.

International Journal of Decision Support System Technology (IJDSST) 13, 16–44.

Szegedy, C., Liu, W., Jia, Y., Sermanet, P., Reed, S., Anguelov, D., Erhan, D., Vanhoucke, V., Rabinovich, A., 2015. Going deeper with convolutions, in: Proceedings of the IEEE conference on computer vision and pattern recognition, pp. 1–9.

Tang, N., Zhao, X., Li, Y., Zhu, D., 2018. Adaptive threshold shearlet transform for surface microseismic data denoising. Journal of Applied Geophysics 153, 64–74.

Tang, S., Wang, J., Tang, C., 2021. Identification of microseismic events in rock engineering by a convolutional neural network combined with an attention mechanism. Rock Mechanics and Rock Engineering 54, 47–69.

Wang, K., Tang, C., Ma, K., Wang, X., Li, Q., 2020. An automatic recognition method of microseismic signals based on s transformation and improved gaussian mixture model. Advances in Civil Engineering 2020.

Wilkins, A.H., Strange, A., Duan, Y., Luo, X., 2020. Identifying microseismic events in a mining scenario using a convolutional neural network. Computers & Geosciences 137, 104418.

Xu, S., Zhang, C., Chen, Z., Li, Y., Liu, J., 2021. Accurate identification of microseismic waveforms based on an improved neural network model. Journal of Applied Geophysics 190, 104343.

Yoon, C.E., O'Reilly, O., Bergen, K.J., Beroza, G.C., 2015. Earthquake detection through computationally efficient similarity search. Science advances 1, e1501057.

Zengin, E., Abrahamson, N., 2020. Conditional ground-motion model for damaging characteristics of near-fault ground motions based on instantaneous power. Bulletin of the Seismological Society of America 110, 2828–2842.

Zhang, H., Thurber, C., Rowe, C., 2003. Automatic p-wave arrival detection and picking with multiscale wavelet analysis for single-component recordings. Bulletin of the Seismological Society of America 93, 1904–1912.

Zhang, J., Dong, L., Xu, N., 2020. Noise suppression of microseismic signals via adaptive variational mode decomposition and akaike information criterion. Applied Sciences 10, 3790.

Zhang, J., Jiang, R., Li, B., Xu, N., 2019. An automatic recognition method of microseismic signals based on eemd-svd and elm. Computers & Geosciences 133, 104318.

Zheng, J., Lu, J., Peng, S., Jiang, T., 2018. An automatic microseismic or acoustic emission arrival identification scheme with deep recurrent neural networks. Geophysical Journal International 212, 1389–1397.

Zhu, W., Mousavi, S.M., Beroza, G.C., 2019. Seismic signal denoising and decomposition using deep neural networks. IEEE Transactions on Geoscience and Remote Sensing 57, 9476–9488.